npg

IMMEDIATE COMMUNICATION

Neurotoxic effects of postnatal thimerosal are mouse strain dependent

M Hornig[1], D Chian[1] and WI Lipkin[1,2]

[1]Jerome L and Dawn Greene Infectious Disease Laboratory, Department of Epidemiology, Mailman School of Public Health, Columbia University, New York, NY, USA; [2]Departments of Neurology and Pathology, Columbia University College of Physicians and Surgeons, New York, NY, USA

The developing brain is uniquely susceptible to the neurotoxic hazard posed by mercurials. Host differences in maturation, metabolism, nutrition, sex, and autoimmunity influence outcomes. How population-based variability affects the safety of the ethylmercury-containing vaccine preservative, thimerosal, is unknown. Reported increases in the prevalence of autism, a highly heritable neuropsychiatric condition, are intensifying public focus on environmental exposures such as thimerosal. Immune profiles and family history in autism are frequently consistent with autoimmunity. We hypothesized that autoimmune propensity influences outcomes in mice following thimerosal challenges that mimic routine childhood immunizations. Autoimmune disease-sensitive SJL/J mice showed growth delay; reduced locomotion; exaggerated response to novelty; and densely packed, hyperchromic hippocampal neurons with altered glutamate receptors and transporters. Strains resistant to autoimmunity, C57BL/6J and BALB/cJ, were not susceptible. These findings implicate genetic influences and provide a model for investigating thimerosal-related neurotoxicity.
Molecular Psychiatry advance online publication, 8 June 2004; doi:10.1038/sj.mp.4001529

Keywords: autistic disorder; thimerosal; neurotoxicity; autoimmunity; inbred mouse strains

Autism spectrum disorders (ASDs) comprise a set of highly heritable conditions[1] with core impairments in social interaction, communication, and imagination. The prevalence of ASDs is reported to be rising worldwide,[2–4] an increase not fully explained by changes in awareness and diagnostic patterns.[2,3,5,6] Environmental susceptibility genes may be determinants of adverse neurodevelopmental outcomes following pre- or postnatal exposures. One environmental factor may be increased mercury burden through industrial sources, fish, and sodium ethylmercurithiosalicylate (thimerosal), a preservative recently eliminated from many vaccines.[7,8] A large, retrospective study investigating the association of thimerosal-containing vaccines and neurodevelopmental outcomes in an unselected cohort was inconclusive and called for further research into vulnerability factors.[9] An autoimmune diathesis is described in ASD probands[10–15] and their first degree relatives.[16,17] Major histocompatibility complex (MHC) genes regulate risk of mercury-induced autoimmunity in mice.[18,19] To examine whether immunogenetic factors mediate vulnerability to mercury-related neurodevelopmental damage, we exposed mice of differing MHC (H-2) backgrounds[20] to thimerosal in doses and timing equivalent to the pediatric immunization schedule. Profound behavioral and neuropathologic disturbances were observed after postnatal thimerosal in SJL/J (H-2^s) mice, but not in strains without autoimmune sensitivity (BALB/cJ, H-2^d, or C57BL/6J, H-2^b mice).

Materials and methods

Animals

Mouse pups of SJL/J (SJL), C57BL6/J (C57), and BALB/cJ (BALB) strains (Jackson Labs) were inoculated intramuscularly (i.m.) at postnatal day (P)7, P9, P11, and P15 with: (1) *thimerosal-only* (*Thim-only*), 14.2, 10.8, 9.2, or 5.6 μg/kg of ethylmercury per postnatal immunization day, respectively, as sodium ethylmercurithiosalicylate (Sigma); (2) *thimerosal-vaccine* (*Thim-vax*), thimerosal-preserved Diphtheria, Tetanus, acellular Pertussis (DTaP, Lederle), and Haemophilus influenza B (HiB, Lederle) vaccines; or (3) *Control* (phosphate-buffered saline (PBS)) in 25–50 μl volume. Administration days were based on the 2001 US immunization schedule:[7] two, four, six, and 12 months of age. Differences between human and murine central nervous[21] and immune system[22] maturation, including neuronal migration and window of immune tolerance, guided time point selection. P7 in mice is expected to be after most neuronal migration has occurred, but before cerebellar,[21] hippocampal,[21] and amygdalar[23] maturation

Table 1 Development of mouse equivalents of dosage and timing of US 2001 recommended childhood immunization schedule

	Age of infant (in months)			
	2	4	6	12
Mouse postnatal age equivalent	Day 7	Day 9	Day 11	Day 15
EtHg load (μg)	62.5	62.5	62.5	50.0
10th percentile weight (US boys—2000, in kg)	4.4	5.8	6.8	9.0
EtHg dose (μg/kg)	14.2	10.8	9.2	5.6
Thimerosal-preserved vaccines administered at each age according to US Immunization Schedule (μg/dose)	Hep B (12.5) DTaP (25) HiB (25) (PCV (25))	Hep B (12.5) DTaP (25) HiB (25) (PCV (25))	Hep B (12.5) DTaP (25) HiB (25) (PCV (25))	— DTaP (25) HiB (25) (PCV (25))

DTaP, Diphtheria–Tetanus–acellular Pertussis; EtHg, ethylmercury; HepB, hepatitis B; HiB, Haemophilus influenza B; PCV, pneumococcal vaccine. PCV is noted within parenthesis to indicate that it was not routinely included in state vaccine requirements.

conclude, thus more closely approximating the maturing human postnatal central nervous system (CNS).[21] Dosages were calibrated to cumulative vaccine ethylmercury burden[7] after adjustment to 10th percentile weights for boys[24] for each age (Table 1). Ethylmercury load in *Thim-vax* group was equivalent to that in *Thim-only* groups, but included DTaP and HiB components. After weaning (week (wk) 3), mice were group-housed with free access to water and food (PicoLab®). Animal experiments were approved by Institutional Animal Care and Use Committees.

Clinical assessments
Mice were assessed for developmental and motor changes (P8, P10), including protoambulatory responses (2-min test, Coulbourn); righting reflex; and negative geotaxis.[25] A maximum of two pups per litter were tested.[26] A minimum of four litters per drug group was used within each strain. Change in weight from preimmunization P7–P15 was calculated for all pups as: (P15 weight−P7 weight)/P7 weight to adjust for maternal litter effects.

Behavioral studies
We assessed open field locomotor, exploratory, and repetitive activities (90-min test, Coulbourn automated chambers) and motor coordination (rotarod, 20 rpm) using tasks appropriate to developmental age and suspected domains of dysfunction[27] at wks 4 and 10. At wks 10–12, mice were administered a 20-min 'hole board test' using a novel 4×4 hole arena (Coulbourn). At 14–24 wks postnatal, 8-day simple spatial learning trials were performed in SJL mice in nose poke arenas, following food restriction to 85% of baseline weight and 20-min habituation (trial day 1). Spatial learning consisted of four 3-min daily trials (north, south, east, or west starting positions) for 6 days, with single baited hole. A probe trial with south starting position and the same baited hole was conducted on day 8. Nose poke time, time to baited hole, task distance, task errors, and reference memory ratio for south direction on each training day were analyzed.

Histology and immunohistochemistry (IHC)
Anesthetized 5-wk-old animals were perfused with PBS followed by 4% buffered paraformaldehyde in 0.1 M phosphate buffer. Coronal brain slices (2 mm) were postfixed in paraformaldehyde at 4°C for 30 min. After cryoprotection in 30% sucrose, serial 14 μm coronal cryostat sections were collected. Coronal sections of dorsal hippocampus, bregma level −1.46 to −1.82 mm,[28] were randomly selected for analysis (three mice per group; SJL and BALB, *Thim-vax*, and *Control* only). Tissue sections were stained with hematoxylin and eosin (H&E) for histological assessment and regional measurements. IHC was performed using the primary polyclonal antibodies: rabbit anti-*N*-methyl-D-aspartate (NMDA) receptor (NR) type 1 (NR1, 1:25 dilution), rabbit anti-NR2B (1:750 dilution, Chemicon); goat anti-kainic acid (KA) type 2 (KA2) receptor (1:50 dilution), goat anti-excitatory amino-acid transporter (EAAT) type 2 (EAAT2, 1:150 dilution), and goat anti-EAAT3 (1:25 dilution, Santa Cruz). Secondary antibodies were biotinylated anti-rabbit or anti-goat IgG (1:200 dilution, Vector Laboratories, Burlingame, CA, USA). Antibody binding was visualized using Vectastain ABC (Vector Laboratories, Burlingame, CA, USA) with diaminobenzidine (DAB) as chromogen. As a control for nonspecific binding, coronal brain sections incubated without primary antibody (secondary antibody only) were included in each immunohistochemical assay for comparison.

To derive unbiased estimates of neuronal density in and size of dorsal hippocampus subregions, averaged measurements of three coronal sections of each brain at matched rostrocaudal levels were derived in blinded manner and used for analysis ($n = 12$; three mice per group). Maximum widths of granule cell layer of supra- and infrapyramidal blades of dentate gyrus (DG); infrapyramidal aspect of molecular layer

(ML) of DG; stratum laconosum-moleculare (*slm*) of cornu ammonis (CA) subregion 1 (CA1); stratum radiatum (*sr*) of CA1 and CA3; stratum lucidum (*sl*); stratum oriens (*so*) of CA1 and CA3; and CA1 pyramidal cell layer (*pcl*, immediately dorsal to the lateral tip of the suprapyramidal blade of DG) were measured manually using digital photomicrographs at $\times 4$ magnification captured with a Nikon E600 microscope (Nikon Spot software version 3.5.7 for Mac OS X). Neuronal density was measured in CA1 *pcl* (number of linearly arranged neurons spanning the measured width of CA1 *pcl* from its rostral to its caudal extent, expressed as number of neurons/μm) using images captured at $\times 50$ in the same region as that used for estimating the width of CA1 *pcl*.

Cerebellar Purkinje cells (PC) were counted in blinded manner in 10 digital photomicrographs of nonoverlapping, linear stretches of PC layer (lobules VI, VII) of H&E-stained brains ($\times 40$ magnification, SJL: *Thim-vax*, $n=3$, *Control*, $n=3$; BALB: *Thim-vax*, $n=5$, *Control*, $n=5$). Cells with fragmented DNA were labeled by TUNEL, using DAB.[29] Positive cells (brown nuclear staining) were counted in five randomly selected fields ($10 \times$ magnification) in the hippocampus.

Statistical analysis
Statview v.5.0.1 software (SAS Institute, Cary, NC, USA) was used for all statistical analyses. Individual thimerosal group means (*Thim-only*, *Thim-vax*) were compared by paired Student's *t*-test; as differences between the two thimerosal groups were not significant, data were pooled for analyses (*Thim*). Homogeneity of variance was established for individual dependent variables by use of variance ratios (F-test) within drug groups, split by strain and by gender, with the level of significance of $\alpha = 0.05$; where significant heterogeneity of variance between groups was detected, and was not addressed by data transformation, nonparametric analyses were pursued. For parametric behavioral data, a three-way analysis of variance (ANOVA) was performed with strain, drug, and sex as between-subjects factors. A nominal level of significance of $\alpha = 0.05$ was adopted and corrected in *post hoc* analyses (Fisher's protected least significant differences test) to keep type-I error <0.05. Where significance was maintained in *post hoc* tests for between-strain effects, a 2×2 ANOVA (between-subjects factors: drug, sex) was performed within strains to determine the pattern of effect. Repeated measures (RM)-ANOVA was performed to assess change in behavioral variables across test session time segments. Three levels were used for the within-subjects factor, 'time segment,' for 90-min sessions (30-min segments); four levels were used for 20-min tests (5-min segments). Strain, drug, and sex were used as between-subjects factors (3, 2, and 2 levels, respectively). Where significant main effects were confirmed by *post hoc* testing, within-strain RM-ANOVA (between-subjects factors: drug, sex; within-subjects factor: time segment) was employed to

ascertain direction of effect. A direct means comparison by unpaired Student's *t*-test defined direction of effect where significant main sex effects were found within strains. Correlations between behavioral parameters were assessed by deriving correlation coefficients, with Fisher's *r* to *z* transformation. For non-Gaussian distributions, nonparametric tests (Mann–Whitney *U*-test, Spearman's rank-correlation test) were used to determine significance levels. To estimate drug effects on brain architecture, neuropathologic measurements were compared within strains using ANOVA with drug as between-subjects factor except in cases of unequal variances, where nonparametric analyses were pursued.

Results

Significant behavioral findings following thimerosal, as a function of mouse strain and sex, are summarized (Table 2).

Thimerosal causes growth retardation in SJL mice
Mice were observed daily beginning at the first inoculation on P7. Through 24 wks no overt disease was observed in any treatment group. The two thimerosal administration groups in each strain (*Thim-only* or mercury-equivalent *Thim-vax*) had no significant differences in any parameters measured; thus, they were combined for analyses as *Thimerosal-treated* (*Thim*) mice. No between-group differences were found in motor performance through P10. Strain-dependent effects were observed in weight gain through P15 (strain: $F[2,241]=4.512$, $P=0.0119$; drug: $F[1,241]=17.687$, $P<0.0001$; strain $\times$ drug: $F[2,241]=4.484$, $P=0.0122$). Within-strain comparisons revealed retarded weight gain in SJL *Thim* mice (drug, SJL: $F[1,137]=40.596$, $P<0.0001$; C57 and BALB: $P=NS$) (Figure 1a).

Thimerosal is associated with hypoactivity in SJL mice in open field environment at 4 wks of age
Total locomotor activity and exploration in the floor (*XY*) and vertical (*Z*) planes were tested at wk 4. Distance traversed over 90 min showed main effects of strain ($F[2,152]=52.251$, $P<0.0001$) and drug ($F[1,152]=5.319$, $P=0.0224$). The between-strain drug effect was not significant on *post hoc* comparison. Within SJL groups, distance was reduced with thimerosal (drug, $F[1,76]=8.662$, $P=0.0043$). No significant effects were noted in C57 or BALB mice (Figure 1b).

To determine whether the reduction in locomotor activity in SJL *Thim* mice at wk 4 differentially affected exploratory and repetitive behaviors, and whether strain-dependent effects on exploratory and stereotypic behaviors confounded measures of total locomotion, we compared ambulatory/exploratory and stereotypic parameters between and within strains in open field. Exploratory rearings (*Z* plane entries) were influenced by strain ($F[2,152]=41.594$, $P<0.0001$); a between-strain drug

4

Table 2 Summary of thimerosal-related behavioral findings by strain and sex

Parameter	Mouse strain					
	SJL		C57		BALB	
	M	F	M	F	M	F
Birth to P10						
Growth	↓	↓	—	—	—	—
Developmental reflexes (through P10)	—	—	—	—	—	—
Week 4						
Open field						
Total distance	↓	↓	—	—	—	—
Exploratory rearing	↓	↓	—	—	—	—
Total ambulatory distance	↓	↓	—	—	—	—
Center ambulatory distance	↓	↓	—	—	—	—
XY plane stereotypy episodes	↓	↓	—	—	—	—
Z plane stereotypy episodes	↓	↓	—	—	—	—
RotaRod	—	—	—	—	—	—
Week 10						
Open field						
Total distance	(↓)	(↓)	—	—	—	—
Exploratory rearing	↓	↓	—	—	—	—
Center ambulatory distance	↓	—	—	—	—	—
Z plane stereotypy episodes	—	—	—	—	—	—
RotaRod	—	—	—	—	—	—
Week 10–12						
Novel environment						
Exploratory rearing	—	—	—	—	—	—
Center ambulatory distance	↑	↑	—	—	—	—
Nose poke time	↑	↓	—	—	—	—
Z plane stereotypy episodes	—	—	—	—	—	—
Week 14–24						
Simple associative spatial learning and memory task	—	—	—	—	—	—

Arrows indicate direction of effect, where significant. Arrows within parentheses indicate direction of nonsignificant trends. —, no significant thimerosal-related within-strain differences for that parameter.

effect (F[1,152] = 4.349, P = 0.0387) was not significant on *post hoc* comparison testing. Within strains, only SJL *Thim* mice had reductions in total rearing count (F[1,76] = 4.903, P = 0.0298) (Figure 1c). Episodes of stereotypic movements in the XY and Z planes at 4 wks were influenced by strain (*XY stereotypy*: F[2,152] = 56.754, P < 0.0001; *Z stereotypy*: F[2,152] = 81.219, P < 0.0001); between-strain drug effects (*XY stereotypy*: F[1,152] = 6.461, P = 0.0120; *Z stereotypy*: F[1,152] = 5.254, P = 0.0233) were not significant on *post hoc* testing. Within strains, SJL *Thim* mice had fewer total episodes of XY and Z plane stereotypy behaviors, with significant main drug effects (*XY stereotypy*: F[1,76] = 7.356, P = 0.0083; *Z stereotypy*: F[1,76] = 9.547, P = 0.0028)

(Figure 1d and e). Total and stereotypic measures were strongly correlated within both the XY ($r^2 = 0.96$, P < 0.0001) and Z ($r^2 = 0.85$, P < 0.0001) planes.

Thimerosal also affected total ambulatory movements and ambulatory distance traveled within the center of the open field in a strain-dependent manner (*ambulatory distance*: F[2,152] = 71.666, P < 0.0001; *ambulatory center distance*: F[2,152] = 30.379, P < 0.0001). Between strains, drug effects (*ambulatory distance*: F[1,152] = 4.814, P = 0.0297; *ambulatory center distance*: F[1,152] = 4.487, P = 0.0358) were not significant on *post hoc* testing. Within strains, there was a main drug effect for SJL mice, with reduced total ambulatory distance (F[1,76] = 11.753, P = 0.0010) and center ambulation distance (F[1,76] = 5.745, P = 0.0190) in SJL *Thim*, but no drug effect in C57 or BALB mice (both P = NS) (Figure 1f and g).

To evaluate whether hypoactivity of SJL *Thim* mice was responsive to environmental adaptation, we examined changes in ambulatory measures as a function of time. RM-ANOVA showed an additional main effect of time and a time × drug interaction effect for SJL mice for ambulatory distance (time, F[2,152] = 259.309, P < 0.0001; time × drug, F[2,152] = 6.042, P = 0.0030), with drug-related reductions in the first (mean ± standard error of the mean (SEM), *Thim vs Control* SJL, 1166.19 ± 57.3 vs 1416.66 ± 32.2, F[1,76] = 15.386, P = 0.0002) and second (*Thim vs Control* SJL, 645.87 ± 56.4 vs 862.61 ± 48.03, F[1,76] = 8.867, P = 0.0039), but not the last 30-min period of the test session (P = NS).

Similarly, within-strain analyses for ambulatory center distance over time revealed a main effect of time for SJL mice only (F[2,152] = 82.589, P < 0.0001), with a trend toward a thimerosal-induced reduction in ambulatory center distance in the first 30 min (*Thim vs Control* SJL, 248.08 ± 26.6 vs 303.46 ± 18.7, F[1,76] = 3.199, P = 0.0777), and a reduction in the second 30 min *Thim vs Control* SJL, 119.37 ± 18.8 vs 183.58 ± 18.2, F[1,76] = 6.202, P = 0.0149).

Thimerosal effects on behavior of SJL mice at wks 10–12 vary with environmental novelty
We evaluated whether strain-dependent alterations in locomotor and exploratory behaviors of *Thim* mice changed at later ages in open field or novel hole board (wks 10–12). At wk 10, we found strain effects, but no overall drug effects, in total distance traversed in the open field (strain, F[2.120] = 66.459, P < 0.0001); however, within-strain comparisons showed only a trend toward a reduction in SJL *Thim* mice (F[1,91] = 2.791, P = 0.0982).

Rearing count in open field showed a strain, but no overall drug effect at wk 10 (strain, F = 104.162, P < 0.0001); within-strain comparisons indicated a main effect of drug only in SJL mice, with reduced rearing counts in SJL *Thim* mice (F = 5.332, P = 0.0232), without sex effect (Figure 2a). Exploratory rearings did not differ in the novel hole board between (data not shown) or within strains (SJL mice, Figure 2b).
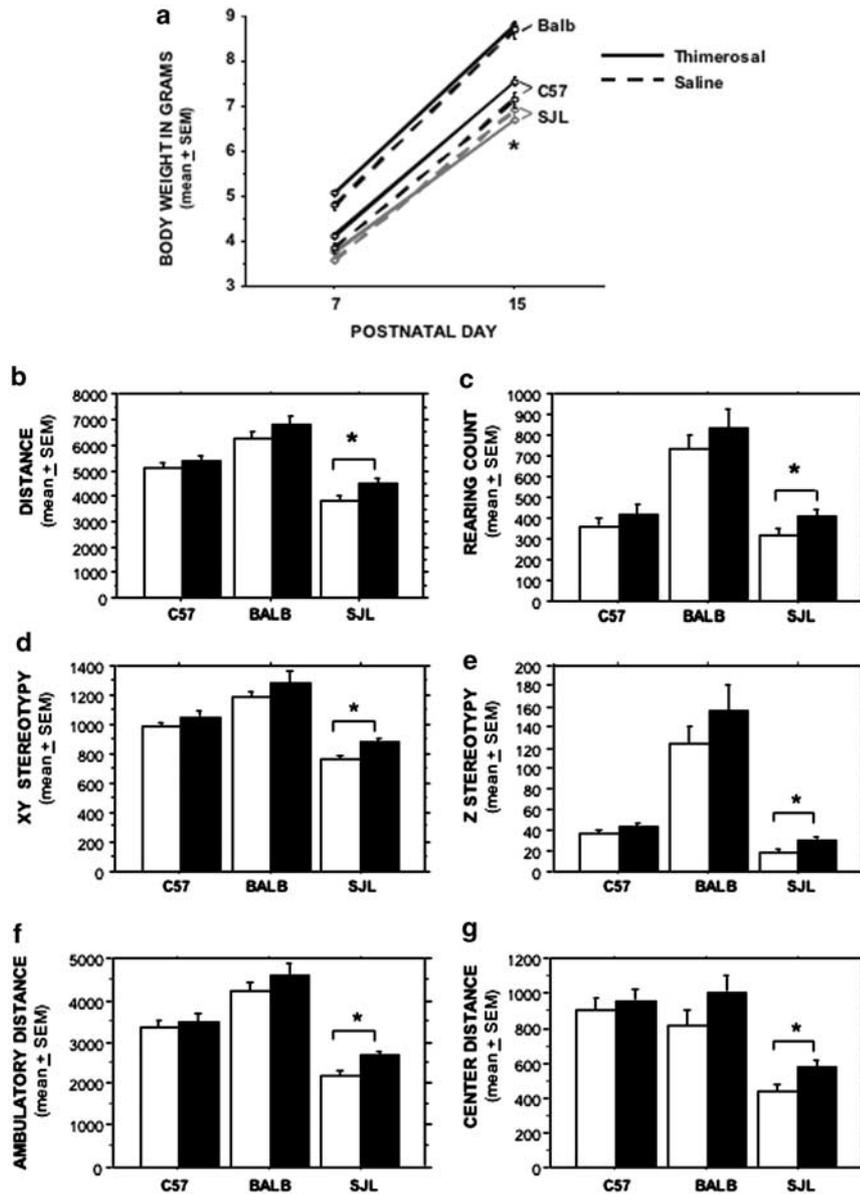
Figure 1 Thimerosal is associated with growth delay and behavioral impoverishment in SJL mice. (a) Solid black lines, BALB and C57 *Thim*; dashed lines, BALB and C57 *Control*. Solid grey line, SJL *Thim*; dashed grey line, SJL *Control*. (b–g) Open bars, *Thim*. Dark bars, *Control*. (a) Weight at preimmunization baseline (P7) and P15. Impairment of weight gain is observed in SJL *Thim* mice (solid grey line, *P* < 0.0001). (b–g) Open field behaviors are reduced at wk 4 in SJL *Thim* vs SJL *Control* mice, including: (b) distance traveled (*P* = 0.0043), (c) rearing counts (*P* = 0.0298), (d) *XY* (floor) plane stereotypy episodes (*P* = 0.0083), (e) *Z* (vertical) plane stereotypy episodes (*P* = 0.0028), (f) total ambulatory distance (*P* = 0.0010), (g) total ambulatory distance traversed through arena center (*P* = 0.0190).

Contrasting strain- and sex-dependent effects of thimerosal were observed in margin-oriented thigmotaxis in open field *vs* hole board. As at wk 4, wk 10 open field total ambulatory center distance was subject to strain effects, but no overall drug effects across strains (strain, F = 48.631, *P* < 0.0001). The main effects of sex were observed for SJL mice on within-strain comparisons (F = 5.269, *P* = 0.0240), and a trend toward a main effect for drug (F = 3.179, *P* = 0.0779). No main effects were noted within other

strains. On direct means comparisons, male SJL *Thim* mice, compared to male SJL *Control* mice, had reduced open field center ambulation distance (males (*n* = 48): *t* = −2.843, *P* = 0.0066; females (*n* = 47): *P* = NS) (Figure 2c).

In the hole board arena, strain (F[2,122] = 35.668, *P* < 0.0001) and drug × sex interaction (F[2,122] = 5.366, *P* = 0.0222) effects were observed in ambulatory center distance. Within strains, there was an increase in ambulatory center distance in SJL *Thim*
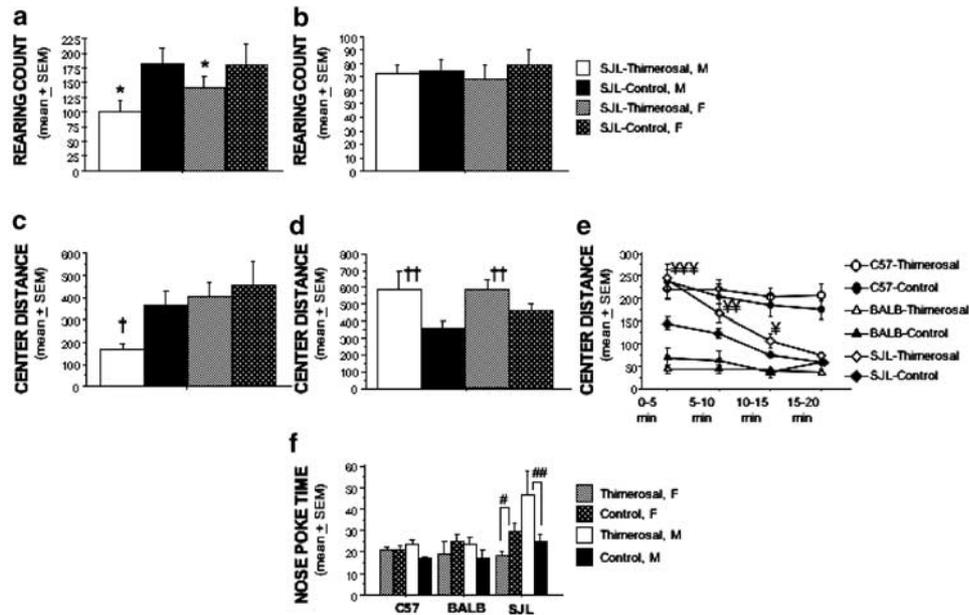
Figure 2 Thimerosal alters responses to open field and novel environments in SJL mice. Open field (a and c). Hole board (b, d, e and f). (a) Rearing counts in open field are decreased in SJL *Thim* mice (SJL *Thim* vs *Control*, *$P = 0.0232$). (b) In hole board, no overall differences in rearing behaviors are observed between drug groups. (c) Ambulatory center distance is decreased in male SJL *Thim* mice in the open field (male SJL *Thim* vs *Control*, †$P = 0.0066$; female SJL *Thim* vs *Control*, $P = $NS). (d) Ambulatory center distance is increased in SJL *Thim* mice in the hole board (SJL *Thim* vs *Control*, ‡$P = 0.0035$). (e) Ambulatory center distance within 5-min segments of the 20-min hole board test session is increased in SJL *Thim* mice in the first (¥¥¥$P = 0.0001$), second (¥¥$P = 0.0300$), and third (¥$P = 0.0355$) 5-min segments relative to *Control* mice. (f) Total nose poke time in the hole board is altered in opposing directions in SJL *Thim* mice as a function of sex, with increases in male SJL *Thim* (##$P = 0.0112$) and decreases in female SJL *Thim* females (#$P = 0.0472$). M, male; F, female.

mice (drug, F[1,63] = 9.185, $P = 0.0035$) (Figure 2d). Ambulatory center distance in the hole board varied over session time as a function of drug in SJL mice, with a main effect of time (F[3,189] = 87.965, $P < 0.0001$) and time × drug interaction effect (F[3,189] = 8.390, $P < 0.0001$). In SJL mice ($n = 67$), the drug effect was especially marked for the first 5 min of the 20-min test session ($t = 4.142$, $P = 0.0001$) and remained significant through the third 5-min segment of the session (5–10 min segment: $t = 2.219$, $P = 0.0300$; 10–15 min segment: $t = 2.172$, $P = 0.0335$; 15–20 min segment: $P = $NS) (Figure 2e).

Exploratory nose poke activity in the hole board was associated with strain (F[2,122] = 6.109, $P = 0.0030$), strain × sex (F[2,122] = 3.293, $P = 0.0405$), and drug × sex (F[1,122] = 9.058, $P = 0.0032$) effects. A drug × sex interaction effect (F[1,63] = 11.899, $P = 0.0010$) was found on within-strain comparisons for SJL mice. A main effect of sex (F[1,63] = 6.787, $P = 0.0114$) did not retain significance on *post hoc* testing, and there was no main, within-strain drug effect. No main or interaction effects were observed for C57 or BALB mice for nose poke time. To pursue the drug × sex interaction, we performed direct means comparisons within SJL groups split by sex and found complex, opposing effects on total nose poke time: significant increases in SJL *Thim* males ($n = 33$, $t = 2.699$, $P = 0.0112$) and smaller, but significant

decreases in total nose poke time in SJL *Thim* females ($n = 34$, $t = -2.064$, $P = 0.0472$) (Figure 2f). This effect appeared to be related to the novelty of the hole board environment, as time engaged in stereotypic behaviors in the vertical plane was not affected by thimerosal between or within strains, showed no sex effect, and was not correlated with total nose poke time ($r^2 = 0.12$, $P = $NS). Total locomotor activity was highly correlated with distance traversed through the center in both the novel environment ($r^2 = 0.91$, $P < 0.0001$) and the open field ($r^2 = 0.89$, $P < 0.0001$) tasks in SJL mice.

Thimerosal does not influence acquisition or retention of a simple spatial memory task
Acquisition of a simple spatial nose poke task was tested at age 14–24 wks in SJL mice (*Thim*, $n = 30$; *Control*, $n = 21$). Drug groups did not differ in latency to finding baited hole, distance traveled during task-related activity, task errors, total nose poke time, or reference memory ratio.

Gross motor coordination is minimally altered following thimerosal
We evaluated the effects of strain and drug on cerebellar dysfunction (rotarod test). At wk 4 (C57: *Thim*, $n = 27$, *Control*, $n = 18$; BALB: *Thim*, $n = 10$, *Control*, $n = 5$; SJL: *Thim*, $n = 55$, *Control*, $n = 49$) and

10 (C57: *Thim*, $n = 5$, *Control*, $n = 8$; BALB: *Thim*, $n = 16$, *Control*, $n = 8$; SJL: *Thim*, $n = 47$, *Control*, $n = 41$), no thimerosal-related differences were observed in rotarod performance between or within strains on accelerating rod (20 rpm).

Hippocampal architecture and glutamate receptor and transporter immunoreactivity are disrupted in SJL mice by postnatal thimerosal

The number and density of neurons were increased in (DG, CA1, and CA2 regions of the hippocampus of SJL *Thim* mice. In CA1, number of neurons through the width of CA1 and the density of those neurons were significantly increased for SJL *Thim* mice, but unaffected by drug in BALB mice (*CA1 neuron number*, mean $\pm$ SEM, SJL: *Thim*, 13.3 ± 0.9, *Control*, 7.3 ± 0.7, $F[1,4] = 29.455$, $P = 0.0056$; BALB: *Thim*, 9.0 ± 1.0, *Control*, 7.7 ± 1.2, $P = NS$; *CA1 neurons/ CA1 width*, number of neurons/μm width of CA1, SJL: *Thim*, 0.143 ± 0.009, *Control*, 0.099 ± 0.003, $F[1,4] = 20.388$, $P = 0.0107$; BALB: *Thim*, 0.177 ± 0.012, *Control*, 0.111 ± 0.023, $P = NS$). Although not densely packed, pyramidal neurons in the CA3

subfield were spread in a wide arc and increased in number. The suprapyramidal blade of DG was distorted to a greater degree than the infrapyramidal blade. The later developing infrapyramidal blade, however, was significantly larger in three of three SJL *Thim* mice (*infrapyramidal DG width* (μm), SJL: *Thim*, 146.0 ± 3.2, *Control*, 95.2 ± 0.0, $F[1,4] = 256.202$, $P < 0.0001$; BALB: *Thim*, 134.9 ± 21.3, *Control*, 142.6 ± 40.7, $P = NS$). In one of three SJL *Thim* mice, the width of the earlier developing suprapyramidal blade was 175% greater than the mean suprapyramidal DG width of SJL *Control* mice. Pyramidal cells of SJL *Thim* CA1 and CA2 subfields, but not CA3, were hyperchromic, but neither hypereosinophilic nor pyknotic (Figure 3a and b). Increases in the width of *so* of CA1 and CA3 were noted in SJL *Thim* mice (CA1 *so*: *Thim*, 213.3 ± 61.3, *Control*, 120.0 ± 5.8, Mann–Whitney, $P = 0.0495$; CA3 *so*: *Thim*, 390.0 ± 56.9, *Control*, 134.3 ± 54.2, $F[1,4] = 10.590$, $P = 0.0312$). The width of *sr* was also greater in subfields CA1/CA2 (*Thim*, 341.3 ± 9.7, *Control*, 288.9 ± 11.1, $F[1,4] = 12.665$, $P = 0.0236$) and at CA3 (*Thim*, 364.6 ± 28.0, *Control*, 235.6 ± 22.5,
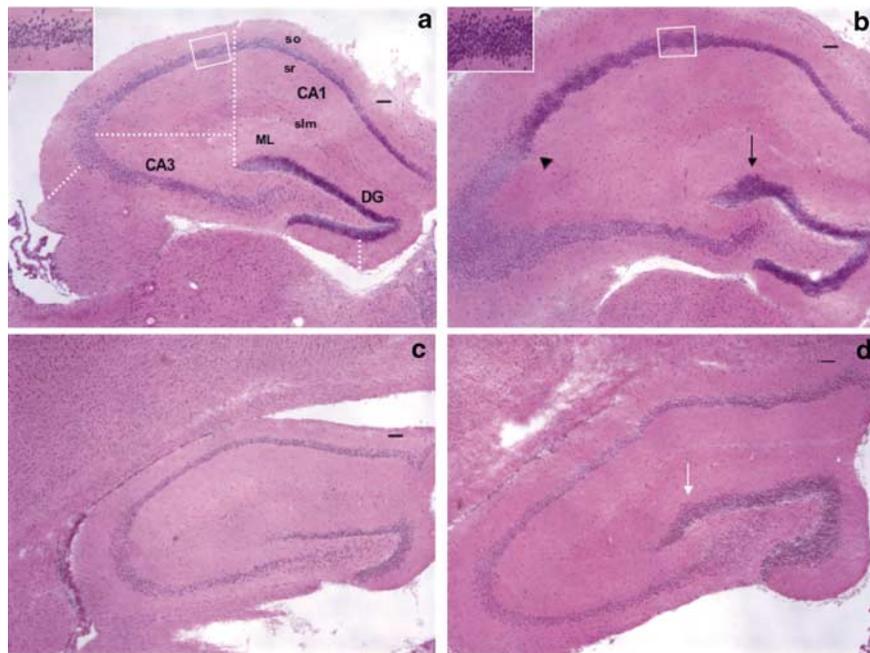

Figure 3 DG and CA regions of the hippocampus are markedly distorted and enlarged in thimerosal-treated SJL mice. Coronal sections of hippocampus at 5 wks postnatal, H&E staining. *DG*, dentate gyrus; *sr*, stratum radiatum; *so*, stratum oriens; *slm*, stratum lacunosum moleculare; ML, molecular layer of DG. Black bars represent 100 μm; white bars, 50 μm. Dotted white lines illustrate relative position of regions selected for measurements within the hippocampal subfields. (a) SJL *Control*. Inset (area of white box) represents CA1 pyramidal cell layer. (b) SJL *Thim-vax*. Increased number and density of neurons in DG, CA1, and CA2 regions of the hippocampus are noted, with distortion of suprapyramidal blade of DG (black arrow). Hyperchromia and increased number and density of pyramidal neurons in CA1 and CA2, without hypereosinophilia or pyknosis, are observed (see inset, area of white box). Pyramidal neurons in CA3 region are distributed in a wide arc and appear increased in number but without change in cell packing density or hyperchromia. A distinct change in cell density and appearance is seen at the presumptive demarcation between CA3 and CA2 subfields (arrowhead). Note larger size of SJL *Thim-vax* hippocampus, including the larger width of *so* and *sr* of both CA1 and CA3 subfields (greater enlargement in CA3 relative to CA1). (c) BALB *Control*. (d) BALB *Thim-vax*. No changes in CA subfields are noted but there is a small increase in number and density of *DG* granule cells (especially notable at suprapyramidal blade, white arrow) without evidence of hyperchromia, and a small increase in the width of *so* in the CA3 subfield.
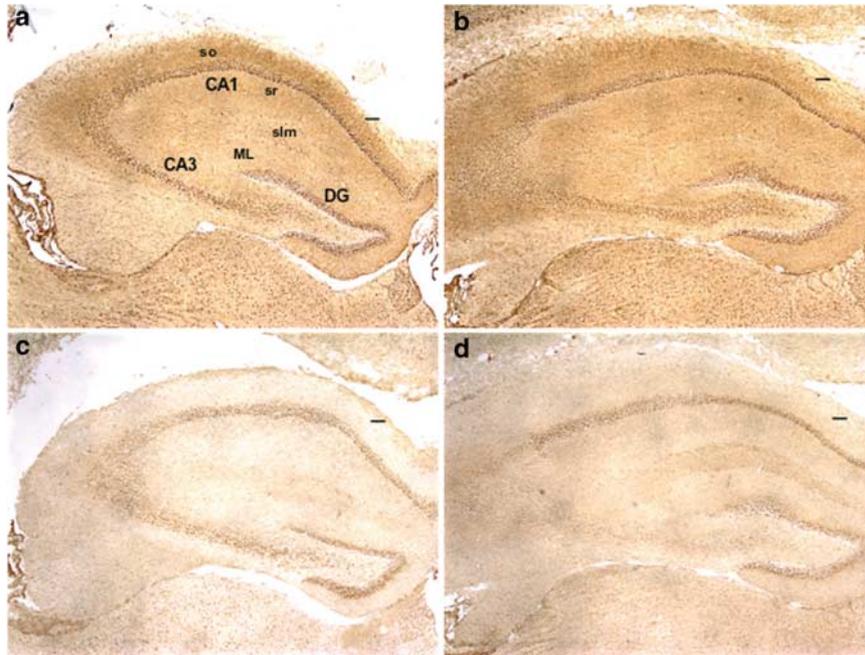
Figure 4 NR1 and NR2b glutamate receptor immunoreactivity patterns are abnormal in the hippocampi of thimerosal-treated SJL mice. Coronal sections of hippocampus, 5 wks PN. (a and c) SJL *Control*; (b and d) SJL *Thim-vax*. (a and b) NR1 IHC; (c and d) NR2b IHC. Black bars represent 100 μm. *DG*, dentate gyrus; *sr*, stratum radiatum; *so*, stratum oriens; *slm*, stratum lacunosum moleculare; ML, molecular layer of DG. (a) SJL *Control*. (b) SJL *Thim-vax*. NR1 receptor immunoreactivity is modestly reduced in SJL *Thim-vax* hippocampus in CA3 pyramidal cell layer relative to that of SJL *Control* in (a). (c) SJL *Control*. (d) SJL *Thim-vax*. NR2b immunostaining is absent in CA3 pyramidal cell layer in SJL *Thim-vax* mice, but not in SJL *Control* (c).

$F[1,4] = 12.900$, $P = 0.0229$). The ratio of CA3/CA1 *sr* width in SJL *Thim* mice was increased, demonstrating a relatively greater lateral enlargement (*Thim*, 1.067 ± 0.061, *Control*, 0.812 ± 0.051, $F[1,4] = 10.149$, $P = 0.0334$). BALB *Thim* mice had no changes in CA subfields relative to BALB *Control*, but showed modest distortion of suprapyramidal DG blade without hyperchromia, and a small increase in size of *so* of the CA3 (*Thim*, 304.8 ± 42.9, *Control*, 225.7 ± 44.4, $F[1,4] = 9.624$, $P = 0.0361$), but not CA1 subfield (Figure 3c and d). No TUNEL-positive cells were detected in the hippocampus or cerebellum of SJL or BALB *Thim* mice at 5 wks. Selected parameters of brain enlargement were correlated with measures of anxiety or reduced tendency to explore that were significantly affected in SJL *Thim* mice: center ambulatory distance during the first 30 min of the wk 4 open field test (*infrapyramidal DG*: $r^2 = -0.829$, $P = 0.0399$; *CA1 neuronal density*: $r^2 = -0.829$, $P = 0.0402$; *CA3/CA1 ratio*: $r^2 = -0.874$, $P = 0.0193$) and exploratory rearing from 0 to 30 min (*CA1 neuronal density*: $r^2 = -0.829$, $P = 0.0404$; *CA3/CA1 ratio*: $r^2 = -0.957$, $P = 0.0009$). These measures were not correlated in BALB mice.

Ionotropic glutamate receptor and transporter immunoreactivity patterns were examined in the hippocampi of *Thim* and *Control* mice. NR1 immunoreactivity was modestly reduced in SJL *Thim* hippocampus in CA3 pyramidal cell layer relative to SJL *Control* (Figure 4a and b). NR2b immunostaining was absent in CA3 pyramidal cell layer in SJL *Thim* mice (Figure 4c and d). KA2 immunoreactivity was reduced in *sr* of the CA1 subfield but increased in *sr* of CA3 (Figure 5a and b). In contrast, KA2 staining was increased in the pyramidal cell layer of CA1 and CA2 relative to CA1 and CA2 pyramidal cell layer in SJL *Control* (Figure 5c and d). Immunostaining in the hippocampus for the glial glutamate transporter, EAAT2, was similar in *Thim* and *Control* mice of both strains at wk 5. In contrast, immunoreactivity patterns for the neuronal glutamate transporter subtype, EAAT3, showed markedly increased EAAT3 staining on the soma of CA1 pyramidal neurons of SJL *Thim* (Figure 6a and b) relative to SJL *Control* mice (insets, Figure 6c and d).

PC counts are reduced in SJL and BALB cerebellum
We examined brains from SJL and BALB mice at wk 5 for the numbers of cerebellar PC (mean of 10, ×40 fields). There was an overall reduction in PC number in *Thim-vax* mice (Mann–Whitney *U*-test, $P = 0.0207$), with nonsignificant trends within strains (SJL *Thim-vax vs Control*, 3.27 ± 0.62 *vs* 4.47 ± 0.29, $P = 0.1266$; BALB *Thim-vax vs Control*, 3.96 ± 0.32 *vs* 4.86 ± 0.33, $P = 0.0758$). The mean PC counts and performance at wk 4 on stationary or rotating rods were not significantly related (Spearman's rank-correlation test).
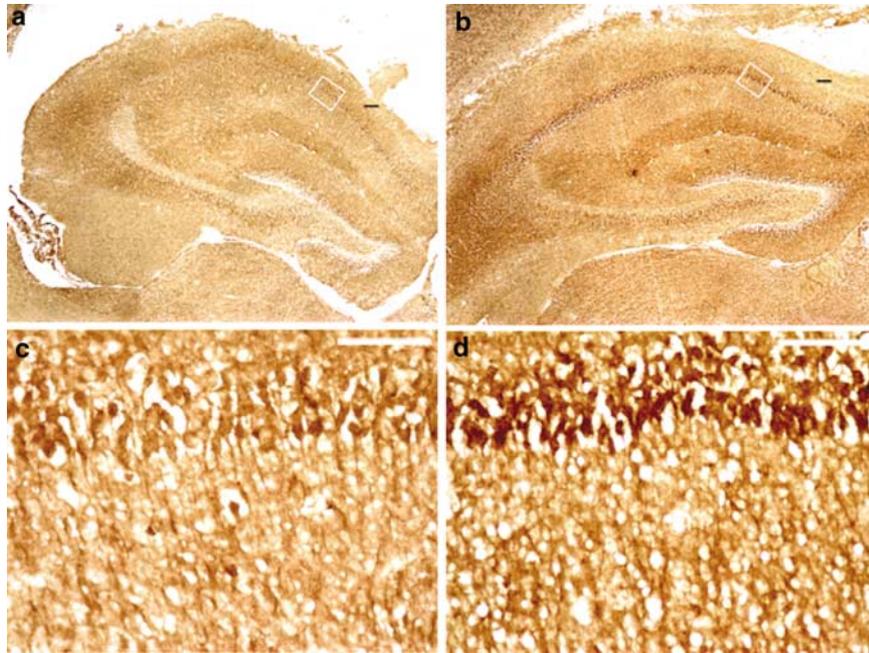
Figure 5 KA2 receptor immunoreactivity patterns are abnormal in the hippocampi of thimerosal-treated SJL mice. Coronal sections of hippocampus, 5 wks PN. (a and c) SJL *Control*, KA2 IHC; (b and d) SJL *Thim-vax*, KA2 IHC. Regions of CA1 represented in (c and d) are marked (white box) in (a and b). *DG*, dentate gyrus; *sr*, stratum radiatum; *pcl*, pyramidal cell layer. Black bars represent 100 μm; white bars, 50 μm. (a) SJL *Control*. Note the relative absence of staining in *pcl* of CA1 subfield. (b) SJL *Thim-vax*. Reduced KA2 immunostaining is noted in *sr* of CA1, with increased staining in *sr* of CA3 and in *pcl* of CA1 and CA2 relative to SJL *Control*. (c) SJL *Control*. Note the parallel orientation of fibers in *sr*. (d) SJL *Thim-vax*. Increased staining is seen on CA1 pyramidal neurons relative to that in SJL *Control*.
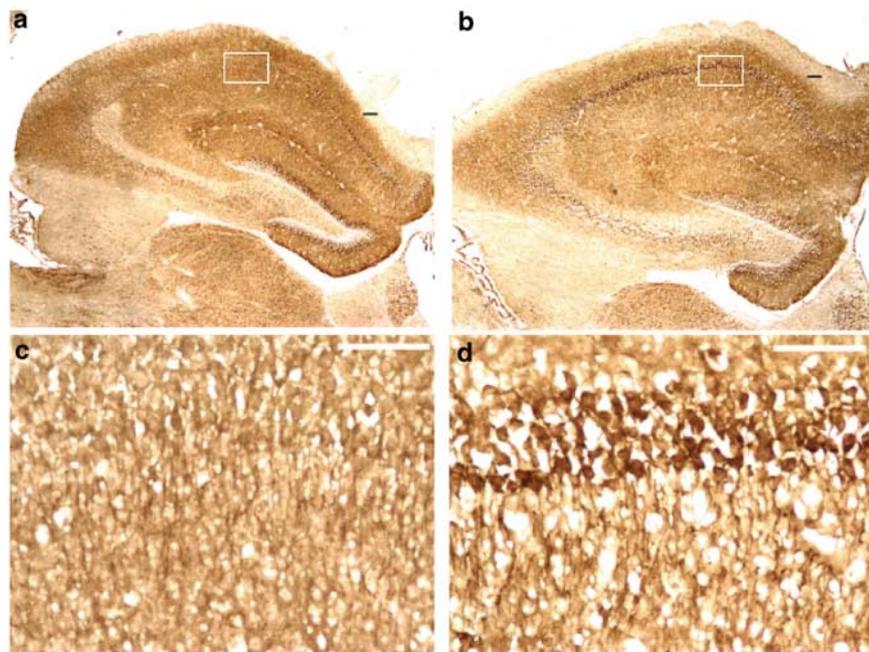

Figure 6 Neuronal glutamate transporter immunoreactivity patterns are abnormal in the hippocampi of thimerosal-treated SJL mice. Coronal sections of hippocampus, 5 wks PN. (a and c) SJL *Control*, EAAT3 IHC; (b and d) SJL *Thim-vax*, EAAT3 IHC. Regions of CA1 represented in (c and d) are marked (white box) in (a and b). Black bars represent 100 μm; white bars, 50 μm. (a) SJL *Control*. (b) SJL *Thim-vax*. Markedly increased EAAT3 staining is noted on the soma of pyramidal neurons in CA1 *pcl* relative to SJL *Control* mice. (c) SJL *Control*. (d) SJL *Thim-vax*. CA1 pyramidal neurons show intense staining on cell bodies.

10

Discussion

The heightened susceptibility of the developing nervous system to mercury is well established, but little is known about factors that modulate sensitivity to repeated, low-dose exposures delivered i.m. or restricted to postnatal life. Although individual differences in maturational timetables, metabolism, nutrition, sex, and immune responses are linked to mercury-induced neurodevelopmental outcomes,[8] most data are based on prenatal, chronic, and/or oral exposures to mercury species other than ethylmercury, in doses exceeding those in the current study. Two primate studies, one in infant humans[30] and another in nonhuman primates,[31] suggest shorter elimination half-lives for vaccine-based thimerosal in both blood and brain than for methylmercury. The slightly higher brain-to-blood partition ratios reported for thimerosal than for methylmercury in the primate study,[31] however, stand in contrast to findings in rats demonstrating higher blood than brain levels following ethyl- than after methylmercury,[32] raising concerns about the ability to predict exposures accurately across mammalian species, developmental stages, or routes or forms of administration.[33] Comparisons of the toxicokinetics of oral methylmercury with i.m. thimerosal exposure in the neonatal *Rhesus* macaque study could not control for differences in the relative maturity of gastrointestinal, immune, and nervous systems and their impact on blood and brain total mercury levels.[33] The human study was not designed to measure pharmacokinetic parameters and missed important early sampling times, leading to possible underestimates of maximal infant exposures. Neither study had sample size sufficient to investigate toxicity as a function of heritable influences. Increased inorganic mercury is observed in all tissues after ethylmercury relative to methylmercury, and is associated with greater growth retardation and renal toxicity than equimolar doses of methylmercury.[32]

Extrapolation from methylmercury studies to ethylmercury or thimerosal may be further limited by differences in immune responses following these alternate forms of organic mercury. Consistent with studies showing elevated inorganic mercury accumulation following ethylmercury, a recent study in A.SW mice, another H-2^s mouse strain vulnerable to mercury-induced autoimmune disturbances, indicates that immune parameters following oral thimerosal in adult animals are more similar to those seen after inorganic mercury than after methylmercury, with elevations of serum IgE, IgG1, IgG2a, and antifibrillarin antibodies.[34] Unfortunately, it is not possible to predict from those data the threshold for risk from repetitive, i.m. thimerosal administration to developing postnatal organisms. The mouse strains compared here were selected for differences in vulnerability to mercury-induced autoimmunity, in a manner linked closely to H-2 genes.[18,19,35–39] Our data suggest that genes linked to autoimmunity, in

general, and to mercury-induced autoimmunity, in particular, may influence the relative neuro- or immunotoxicity of thimerosal.

Our studies have not excluded alternate, non-MHC, strain-dependent mechanisms of thimerosal toxicity. Genes outside the H-2 region influence both the autoimmune sequelae associated with mercury[40] and its toxicokinetics.[40–42] We compared three mouse strains with differing H-2 and non-H-2 backgrounds; such modulatory genetic factors might have been obscured. Variation in toxicokinetics across strains may alter distribution, retention, or rates of metabolism from organic to inorganic mercury species.[40,41,43] Toxicokinetic explanations, however, predict lower thresholds for the induction of autoimmune disturbance following mercury administration to females of H-2-susceptible strains.[40] Here, we found no sex-related effects on behavior at prepubertal time points in susceptible SJL mice, and only few postpubertally; in these instances, males were more significantly affected than females. The administration of mercury at early postnatal ages is not associated with sex differences in distribution or excretion.[44] The differences we observed in older female and male SJL mice in response to open field and novel environment may result from the impact of sex hormones on neural circuitry already disrupted through earlier mercury exposure.

Further, immune response genes may be linked to other heritable factors mediating toxin-induced CNS damage, such as systems regulating antioxidant[45] or DNA methylation[46] status, apoptosis pathways,[47] glutamatergic transmission or excitotoxicity,[48] metallothionein isoforms,[49] or proinflammatory cytokine responses.[50] As a central role is implicated for the Th1-type cytokine, interferon-γ (IFN-γ), in mercury-induced autoimmunity[51] and general autoimmune disease susceptibility,[52] we included C57 mice in our strain comparison; similar to SJL mice, C57 mice show a Th1-type cytokine predominance, including increased levels of IFN-γ gene expression at baseline,[53] yet are less sensitive than SJL mice to autoimmune sequelae following mercury or other Th1-dependent, autoimmunity-provoking challenges.[54,55] BALB mice, in contrast, demonstrate predominance of Th2-type cytokines, with reduced basal levels of transcripts representing IFN-γ relative to C57 and SJL mice,[53] and resistance to Th1-initiated autoimmune diseases.[56] The susceptibility to the neurotoxic effects of low-dose postnatal thimerosal closely paralleled these immune vulnerabilities.

We introduced thimerosal beginning at P7, a time critical for synaptogenesis and maturation of glutamatergic and other neural pathways,[57] yet after migrational events are largely concluded.[21] In humans, this period of synaptic plasticity extends from the 6th month of gestation to several years after birth and parallels the sensitivity of the developing brain to xenobiotics;[58] NMDA receptors play a key role in these developmental events.[59] Whereas in mature rodents excessive glutamate is neurotoxic, neuronal

survival is promoted by glutamate during brain development.[59] Conversely, blockade of NMDA receptors during the postnatal brain growth spurt (approximately P7–14 in rats) is associated with enhanced neuronal apoptosis.[58,59] It is intriguing to consider that in the context of synaptogenesis, abnormal activation of NMDA receptors may result in the persistence of neurons that might otherwise be selected for developmentally appropriate pruning. Such alterations could explain both our findings of increased numbers of hyperchromic, tightly packed but TUNEL-negative pyramidal neurons in CA1 and CA2, as well as the generalized enlargement of hippocampal structures. These findings are reminiscent of Rett syndrome, a disorder with clinical features overlapping with those of autism but caused by mutations in the X-linked methyl-CpG-binding protein 2,[60] where CA1 pyramidal neurons of increased cell packing density, without evidence of active degeneration[61] and with hyperchromic appearance,[62] are reported. Age-associated brain overgrowth is also noted in autism.[63] Our findings in SJL *Thim* mice not only of significant, selective brain enlargement but also of close, inverse correlations between these histopathologic measures and measures of disinhibition or exploratory drive (center ambulatory distance and exploratory rearing) underscore the relevance of this model for understanding the mechanisms underlying the strain dependent vulnerability of developing neurobehavioral circuitry to neurotoxic insults. The relatively greater increase in *sr* of CA3 than in that of CA1 in SJL *Thim* mice is particularly intriguing. In addition to more general findings of macrocephaly, eurycephaly is reported in children with autism.[64] Of further interest, the infrapyramidal mossy fiber bundle, pruned from up to two-thirds the length of CA3 to its shorter adult length between PN days 20 and 30 in mice,[65] varies genetically and its size is linked to exploratory behaviors.[66] The finding here of a correlation between enlargement of specific regional hippocampal fields and decreased levels of exploration (i.e., reduced center ambulatory distance and rearing counts, consistent with increased anxiety levels) in thimerosal-treated SJL mice suggests that pruning mechanisms may be selectively disrupted by this postnatal challenge. Partial deafferentation effects, with enhanced activity, may also contribute to interrelated abnormalities of DG and region CA1/CA2 abnormalities through incomplete damage to perforant path afferents or Schaffer collaterals. This investigation focused on brain regions that undergo postnatal maturation and are known to be susceptible to organic mercury exposures during development, hippocampus and cerebellum.[8] Potential contributions from thimerosal-related damage in other brain areas, including entorhinal cortex, frontal cortex, cingulate cortex, thalamus, amygdala, and brainstem, need to be considered.

Whether altered patterns of NR1, NR2b, KA2, and EAAT3 immunoreactivity found in SJL *Thim* mice at wk 5 relate to the cytoarchitectonic disturbances in the hippocampi is unclear. Intriguingly, the increased EAAT3 immunoreactivity on the soma of CA1 SJL *Thim* pyramidal neurons is similar to the intracellular EAAT3 translocation observed in models of KA-induced excitotoxicity, where it is proposed as a protective mechanism that averts excessive uptake of glutamate.[67] In SJL *Thim* mice such spatial reorganization of EAAT3 suggests increased levels of glutamate during hippocampal development. Seizure-related increases in extracellular glutamate are noted in temporal lobe epilepsy, along with elevated levels of EAAT3 in remaining hippocampal neurons,[68] possibly as a compensatory mechanism. The expression of EAAT3 not only in glutamatergic but also in GABAergic neurons,[69,70] as well as some astrocytes,[70] implies that mis-steps in the normal ontogeny of EAAT3 in CA1/CA2 may disrupt both glutamate and GABA synthesis and neurotransmission,[71] critically affecting hippocampal plasticity and enhancing risk for limbic hyperexcitability or seizures. Selectivity for the neuronal EAAT3 transporter subtype, and sparing of the glial glutamate transporter, EAAT2, parallels the normal pattern of expression of these transporters during development. Whereas EAAT3 expression is greater in newborn than in adult brain, EAAT2 expression increases as the brain matures.[72] Time-dependent, complex rearrangements of NMDA and kainate receptors are also noted in models of temporal lobe epilepsy after lesions[73] or kainate.[74] As with EAAT3, levels of the NMDA receptor subtype NR2b are highest at birth and decrease in rats by about wk 4 postnatal; additionally, changes in the molecular diversity of heteromeric NMDA receptor channels are thought to parallel age-dependent decreases in the sensitivity of NMDA receptors to competitive antagonists and reflect changes in glutamatergic plasticity.[75]

The pattern of behavioral and neuropathologic findings described here in SJL mice suggests a strain-dependent, ethylmercury-based disruption of normal programs of neural development and synaptogenesis. These findings implicate genetic influences and maturational factors as critical determinants of postnatal thimerosal-related sequelae and highlight the importance of interactions of gene, environment, and timing in the pathogenesis of neurodevelopmental disorders.

References

1 Risch N, Spiker D, Lotspeich L, Nouri N, Hinds D, Hallmayer J *et al.* A genomic screen of autism: evidence for a multilocus etiology. *Am J Hum Genet* 1999; **65**: 493–507.

12

2 Yeargin-Allsopp M, Rice C, Karapurkar T, Doernberg N, Boyle C, Murphy C. Prevalence of autism in a US metropolitan area. *JAMA* 2003; **289**: 49–55.

3 M.I.N.D Institute. *Report to the Legislature on the Principal Findings from the Epidemiology of Autism in California: A Comprehensive Pilot Study*. UC Davis: Sacramento, CA, 2002.

4 Chakrabarti S, Fombonne E. Pervasive developmental disorders in preschool children. *JAMA* 2001; **285**: 3093–3099.

5 Blaxill MF, Baskin DS, Spitzer WO. Commentary: Blaxill, Baskin, and Spitzer on Croen *et al.* (2002). The changing prevalence of autism in California. *J Autism Dev Disord* 2003; **33**: 223–226.

6 Croen L, Grether J. Response: a response to Blaxill, Baskin, and Spitzer on Croen *et al.* (2002). The changing prevalence of autism in California. *J Autism Dev Disord* 2003; **33**: 227–229.

7 American Academy of Pediatrics Committee on Infectious Diseases. Recommended childhood immunization schedule—United States, January–December 2001. *Pediatrics* 2001; **107**: 202–204.

8 Committee on the Toxicological Effects of Methylmercury, Board on Environmental Studies and Toxicology, National Research Council. *Toxicological Effects of Methylmercury*. National Academies Press: Washington, DC, 2000.

9 Verstraeten T, Davis RL, DeStefano F, Lieu TA, Rhodes PH, Black SB *et al.* Safety of thimerosal-containing vaccines: a two-phased study of computerized health maintenance organization databases. *Pediatrics* 2003; **112**: 1039–1048.

10 Connolly AM, Chez MG, Pestronk A, Arnold ST, Mehta S, Deuel RK. Serum autoantibodies to brain in Landau–Kleffner variant, autism, and other neurologic disorders. *J Pediatrics* 1999; **134**: 607–613.

11 Vojdani A, Pangborn JB, Vojdani E, Cooper EL. Infections, toxic chemicals and dietary peptides binding to lymphocyte receptors and tissue enzymes are major instigators of autoimmunity in autism. *Int J Immunopathol Pharmacol* 2003; **16**: 189–199.

12 Singh VK, Warren RP, Odell JD, Warren WL, Cole P. Antibodies to myelin basic protein in children with autistic behavior. *Brain Behav Immun* 1993; **7**: 93–103.

13 Warren RP, Odell JD, Warren WL, Burger RA, Maciulis A, Daniels WW *et al.* Strong association of the third hypervariable region of HLA-DR beta 1 with autism. *J Neuroimmunol* 1996; **67**: 97–102.

14 Torres AR, Maciulis A, Stubbs EG, Cutler A, Odell D. The transmission disequilibrium test suggests that HLA-DR4 and DR13 are linked to autism spectrum disorder. *Hum Immunol* 2002; **63**: 311–316.

15 Warren RP, Yonk J, Burger RW, Odell D, Warren WL. DR-positive T cells in autism: association with decreased plasma levels of the complement C4B protein. *Neuropsychobiology* 1995; **31**: 53–57.

16 Sweeten TL, Bowyer SL, Posey DJ, Halberstadt GM, McDougle CJ. Increased prevalence of familial autoimmunity in probands with pervasive developmental disorders. *Pediatrics* 2003; **112**: e420.

17 Comi AM, Zimmerman AW, Frye VH, Law PA, Peeden JN. Familial clustering of autoimmune disorders and evaluation of medical risk factors in autism. *J Child Neurol* 1999; **14**: 388–394.

18 Hultman P, Hansson-Georgiadis H. Methyl mercury-induced autoimmunity in mice. *Toxicol Appl Pharmacol* 1999; **154**: 203–211.

19 Abedi-Valugerdi M, Möller G. Contribution of H-2 and non-H-2 genes in the control of mercury-induced autoimmunity. *Int Immunol* 2000; **12**: 1425–1430.

20 Klein J, Benoist C, David CS, Demant P, Lindahl KF, Flaherty L *et al.* Revised nomenclature of mouse H-2 genes. *Immunogenetics* 1990; **32**: 147–149.

21 Rice D, Barone SJ. Critical periods of vulnerability for the developing nervous system: evidence from humans and animal models. *Environ Health Perspect* 2000; **108**: 511–533.

22 Holladay SD, Smialowicz RJ. Development of the murine and human immune system: differential effects of immunotoxicants depend on time of exposure. *Environ Health Perspect* 2000; **108**: 463–473.

23 Fink GR, Zilles K, Schleicher A. Postnatal development of forebrain regions in the autoimmune NZB-mouse. A model for degeneration in neuronal systems. *Anat Embryol (Berl)* 1991; **183**: 579–588.

24 National Center for Health Statistics. *Birth to 36 Months: Boys Length-for-Age and Weight-for-Age Percentiles*. CDC: Atlanta, GA, 2000.

25 Altman J, Sudarshan K. Postnatal development of locomotion in the laboratory rat. *Anim Behav* 1975; **23**: 896–920.

26 Holson RR, Pearce B. Principle and pitfalls in the analysis of prenatal treatment effects in multiparous species. *Neurotoxicol Teratol* 1992; **14**: 221–228.

27 Cory-Slechta DA, Crofton KM, Foran JA, Ross JF, Sheets LP, Weiss B *et al.* Methods to identify and characterize developmental neurotoxicity for human health risk assessment. I: Behavioral effects. *Environ Health Perspect* 2001; **109**(Suppl 1): 79–91.

28 Paxinos G, Franklin KBJ. *The Mouse Brain in Stereotaxic Coordinates*. Academic Press: San Diego, CA, 2001.

29 Gavrieli Y, Sherman Y, Ben-Sasson SA. Identification of programmed cell death *in situ* via specific labeling of nuclear DNA fragmentation. *J Cell Biol* 1992; **119**: 493–501.

30 Pichichero ME, Cernichiari E, Lopreiato J, Treanor J. Mercury concentrations and metabolism in infants receiving vaccines containing thiomersal: a descriptive study. *Lancet* 2002; **360**: 1737–1741.

31 Sager PR. Evaluation of thimerosal-containing vaccines in non-human primates. *Presentation at CDC, ACIP Meeting*, 19 June 2003.

32 Magos L, Brown AW, Sparrow S, Bailey E, Snowden RT, Skipp WR. The comparative toxicology of ethyl- and methylmercury. *Arch Toxicol* 1985; **57**: 260–267.

33 Oskarsson A, Palminger Hallen I, Sundberg J, Petersson Grawe K. Risk assessment in relation to neonatal metal exposure. *Analyst* 1998; **123**: 19–23.

34 Havarinasab S, Lambertsson L, Qvarnstrom J, Hultman P. Dose–response study of thimerosal-induced murine systemic autoimmunity. *Toxicol Appl Pharmacol* 2004; **194**: 169–179.

35 Hultman P, Bell LJ, Enestrom S, Pollard KM. Murine susceptibility to mercury. I. Autoantibody profiles and systemic immune deposits in inbred, congenic, and intra-H-2 recombinant strains. *Clin Immunol Immunopathol* 1992; **65**: 98–109.

36 Hultman P, Bell LJ, Enestrom S, Pollard KM. Murine susceptibility to mercury. II. Autoantibody profiles and renal immune deposits in hybrid, backcross, and H-2d congenic mice. *Clin Immunol Immunopathol* 1993; **68**: 9–20.

37 Hanley GA, Schiffenbauer J, Sobel ES. Resistance to HgCl$_2$-induced autoimmunity in haplotype–heterozygous mice is an intrinsic property of B cells. *J Immunol* 1998; **161**: 1778–1785.

38 Johansson U, Hansson-Georgiadis H, Hultman P. The genotype determines the B cell response in mercury-treated mice. *Int Arch Allergy Immunol* 1998; **116**: 295–305.

39 Pollard KM, Pearson DL, Hultman P, Deane TN, Lindh U, Kono DH. Xenobiotic acceleration of idiopathic systemic autoimmunity in lupus-prone BXSB mice. *Environ Health Perspect* 2001; **109**: 27–33.

40 Nielsen JB, Hultman P. Mercury-induced autoimmunity in mice. *Environ Health Perspect* 2002; **110**(Suppl 5): 877–881.

41 Nielsen JB. Toxicokinetics of mercuric chloride and methylmercuric chloride in mice. *J Toxicol Environ Health* 1992; **37**: 85–122.

42 Hultman P, Nielsen JB. The effect of toxicokinetics on murine mercury-induced autoimmunity. *Environ Res* 1998; **77**: 141–148.

43 Nielsen JB, Andersen O. Methyl mercuric chloride toxicokinetics in mice. I: Effects of strain, sex, route of administration and dose. *Pharmacol Toxicol* 1991; **68**: 201–207.

44 Hirayama K, Yasutake A. Sex and age differences in mercury distribution and excretion in methylmercury-administered mice. *J Toxicol Environ Health* 1986; **18**: 49–60.

45 Westphal GA, Schnuch A, Schulz TG, Reich K, Aberer W, Brasch J *et al.* Homozygous gene deletions of the glutathione *S*-transferases M1 and T1 are associated with thimerosal sensitization. *Int Arch Occup Environ Health* 2000; **73**: 384–388.

46 Waly M, Olteanu H, Banerjee R, Choi SW, Mason JB, Parker BS *et al.* Activation of methionine synthase by insulin-like growth factor-1 and dopamine: a target for neurodevelopmental toxins and thimerosal. *Mol Psychiatry* 2004; **9**: 358–370.

47 Maas K, Chan S, Parker J, Slater A, Moore J, Olsen N *et al.* Cutting edge: molecular portrait of human autoimmune disease. *J Immunol* 2002; **169**: 5–9.

48 Schauwecker PE. Modulation of cell death by mouse genotype: differential vulnerability to excitatory amino acid-induced lesions. *Exp Neurol* 2002; **178**: 219–235.

49 Espejo C, Carrasco J, Hidalgo J, Penkowa M, Garcia A, Saez-Torres I *et al.* Differential expression of metallothioneins in the CNS of mice with experimental autoimmune encephalomyelitis. *Neuroscience* 2001; **105**: 1055–1065.

50 Wilson AG, di Giovine FS, Duff GW. Genetics of tumour necrosis factor-alpha in autoimmune, infectious, and neoplastic diseases. *J Inflamm* 1995; **45**: 1–12.

51 Kono DH, Balomenos D, Pearson DL, Park MS, Hildebrandt B, Hultman P *et al.* The prototypic Th2 autoimmunity induced by mercury is dependent on IFN-gamma and not Th1/Th2 imbalance. *J Immunol* 1998; **161**: 234–240.

52 Hill N, Sarvetnick N. Cytokines: promoters and dampeners of autoimmunity. *Curr Opin Immunol* 2002; **14**: 791–797.

53 Charles PC, Weber KS, Cipriani B, Brosnan CF. Cytokine, chemokine and chemokine receptor mRNA expression in different strains of normal mice: implications for establishment of a Th1/Th2 bias. *J Neuroimmunol* 1999; **100**: 64–73.

54 Billiau A, Heremans H, Vandekerckhove F, Dijkmans R, Sobis H, Meulepas E *et al.* Enhancement of experimental allergic encephalomyelitis in mice by antibodies against IFN-gamma. *J Immunol* 1988; **140**: 1506–1510.

55 Butterfield RJ, Sudweeks JD, Blankenhorn EP, Korngold R, Marini JC, Todd JA, Roper RJ, Teuscher C. New genetic loci that control susceptibility and symptoms of experimental allergic encephalomyelitis in inbred mice. *J Immunol* 1998; **161**: 1860–1867.

56 Krakowski M, Owens T. Interferon-gamma confers resistance to experimental allergic encephalomyelitis. *Eur J Immunol* 1996; **26**: 1641–1646.

57 Hafidi A, Hillman DE. Distribution of glutamate receptors GluR 2/3 and NR1 in the developing rat cerebellum. *Neuroscience* 1997; **81**: 427–436.

58 Olney JW. New insights and new issues in developmental neurotoxicology. *Neurotoxicology* 2002; **23**: 659–668.

59 Ikonomidou C, Bosch F, Miksa M, Bittigau P, Vockler J, Dikranian K *et al.* Blockade of NMDA receptors and apoptotic neurodegeneration in the developing brain. *Science* 1999; **283**: 70–74.

60 Amir RE, Van den Veyver IB, Wan M, Tran CQ, Francke U, Zoghbi HY. Rett syndrome is caused by mutations in X-linked MECP2, encoding methyl-CpG-binding protein 2. *Nat Genet* 1999; **23**: 185–188.

61 Bauman ML, Kemper TL, Arin DM. Microscopic observations of the brain in Rett syndrome. *Neuropediatrics* 1995; **26**: 105–108.

62 Leontovich TA, Mukhina JK, Fedorov AA, Belichenko PV. Morphological study of the entorhinal cortex, hippocampal formation, and basal ganglia in Rett syndrome patients. *Neurobiol Dis* 1999; **6**: 77–91.

63 Courchesne E, Karns CM, Davis HR, Ziccardi R, Carper RA, Tigue ZD *et al.* Unusual brain growth patterns in early life in patients with autistic disorder: an MRI study. *Neurology* 2001; **57**: 245–254.

64 Deutsch CK, Saunders E, Lauer EA, Joseph R, Tager-Flusberg H. Quantitative assessment of craniofacial dysmorphology in autism and SLI. *Presentation at International Meeting for Autism Research*. Orlando, FL, Vol. 2, 2002; 44.

65 Kantor DB, Kolodkin AL. Curbing the excesses of youth: molecular insights into axonal pruning. *Neuron* 2003; **38**: 849–852.

66 Crusio WE. Genetic dissection of mouse exploratory behaviour. *Behav Brain Res* 2001; **125**: 127–132.

67 Furuta A, Noda M, Suzuki SO, Goto Y, Kanahori Y, Rothstein JD *et al.* Translocation of glutamate transporter subtype excitatory amino acid carrier 1 protein in kainic acid-induced rat epilepsy. *Am J Pathol* 2003; **163**: 779–787.

68 Proper EA, Hoogland G, Kappen SM, Jansen GH, Rensen MG, Schrama LH *et al.* Distribution of glutamate transporters in the hippocampus of patients with pharmaco-resistant temporal lobe epilepsy. *Brain* 2002; **125**: 32–43.

69 Rothstein JD, Martin L, Levey AI, Dykes-Hoberg M, Jin L, Wu D *et al.* Localization of neuronal and glial glutamate transporters. *Neuron* 1994; **13**: 713–725.

70 Conti F, DeBiasi S, Minelli A, Rothstein JD, Melone M. EAAC1, a high-affinity glutamate transporter, is localized to astrocytes and GABAergic neurons besides pyramidal cells in the rat cerebral cortex. *Cereb Cortex* 1998; **8**: 108–116.

71 Sepkuty JP, Cohen AS, Eccles C, Rafiq A, Behar K, Ganel R *et al.* A neuronal glutamate transporter contributes to neurotransmitter GABA synthesis and epilepsy. *J Neurosci* 2002; **22**: 6372–6379.

72 Furuta A, Rothstein JD, Martin LJ. Glutamate transporter protein subtypes are expressed differentially during rat CNS development. *J Neurosci* 1997; **17**: 8363–8375.

73 Geddes JW, Brunner L, Cotman CW, Buzsaki G. Alterations in [³H]kainate and N-methyl-D-aspartate-sensitive L-[³H]-glutamate binding in the rat hippocampal formation following fimbria–fornix lesions. *Exp Neurol* 1992; **115**: 271–281.

74 Franck JE, Kunkel DD, Baskin DG, Schwartzkroin PA. Inhibition in kainate-lesioned hyperexcitable hippocampi: physiologic, autoradiographic, and immunocytochemical observations. *J Neurosci* 1988; **8**: 1991–2002.

75 Brady RJ, Gorter JA, Monroe MT, Swann JW. Developmental alterations in the sensitivity of hippocampal NMDA receptors to AP5. *Brain Res Dev Brain Res* 1994; **83**: 190–196.